Available online at www.sciencedirect.com
ScienceDirect
Ceramics International 37 (2011) 1485–1492
CERAMICS INTERNATIONAL
www.elsevier.com/locate/ceramint

Sintering behaviour and properties of YAlSiO and YAlSiON glass-ceramics

M.A. Sainz *, P. Miranzo, M.I. Osendi

Institute of Ceramics and Glass, CSIC, C/ Kelsen 5, 28049 Madrid, Spain

Received 11 October 2010; received in revised form 25 November 2010; accepted 12 December 2010
Available online 22 January 2011

Abstract

Four different YAlSiO and YAlSiON compositions that produced either glass or glass-ceramic materials were designed. Densities, glass transition temperatures, coefficients of thermal expansion and hardness data were established for each material. The sintering behavior was determined from the hot stage microscopy (HSM) runs. For the YAlSiO glass compositions, the viscosity–temperature curves were estimated from five characteristic HSM points using Scholze's method. The YAlSiON glass-ceramics with higher Y content showed $YAlO_3$ and $SiAl_6O_2N_6$ crystals and the poorer Y composition had crystalline precipitates of Si_3N_4, $Si_4Al_2O_2N_6$ and Y_2SiAlO_5N. The effects of the Al/Si and Y/Si ratios, and the nitrogen content on the properties have been discussed. These glass-ceramics showed relatively high thermal expansion coefficient and hardness and, therefore, its application as protective coatings for metallic components against high temperatures and/or corrosive environments is envisaged.

Keywords: A. Sintering; C. Viscosity, hot stage microscopy; D. YAlSiO glass; D. YAlSiON glass-ceramics

1. Introduction.

Yttrium aluminosilicate (YAlSiO) glasses are known for their high glass transition temperatures and good chemical corrosion resistance [1–5], together with their high values of hardness and elastic modulus [6,7], optical properties and desirable environmental stability [8] over a wide range of compositions. Because of their high glass transition temperatures, moderate thermal expansion coefficients, very low electrical conductivities and high viscosity, YAlSiO glasses have been attempted for replacing current borosilicate glasses used as sealing glass for tungsten and molybdenum joints [2]. Some compositions have also been tested as corrosion resistance glass fibers [9] due to their chemical inertness [1–7]. Present authors [10] have recently succeeded in producing firmly attached glass coatings on stainless steel by flame spraying the raw powders compositions.

Most published data [11–15] indicated that by introducing N atoms in the YAlSiO glass network further rises of hardness, glass transition temperature, density and viscosity occurred. Besides, the addition of small amounts of Si_3N_4 to YAlSiO glasses and the subsequent annealing at 1000–1200 °C led to the partial nucleation of Si_2N_2O, $Y_2Si_2O_7$, and YAG [11,15,16] phases, with the corresponding improvement in some of their properties.

Furthermore, yttrium aluminosilicate glassy compounds containing a little nitrogen are the typical grain boundary compositions of sintered Si_3N_4-based ceramics, which usually dictates their mechanical properties at high temperatures [17–22]. In this case, viscosity is a critical parameter. For self-joining of silicon nitride or even for ceramics-to-metals joining, the knowledge of the hardness and viscosity figures of those oxynitrides glass interlayers is of crucial importance as well [16,23–26].

The direct measurement of viscosity in YAlSiO glasses from the transformation interval to the molten state requires procedures that involve either sophisticated equipment [27] or large specimens if indirect methods [28] are used. Due to their high liquidus temperature, the usual method of measuring viscosities by rotation in the melted glass is not practical. In fact, direct methods [27] data on yttrium aluminosilicate and oxynitride glasses are scarce and, instead, the creep response under compression of bulk glasses [13,28–30] has often been used for determining viscosities in the 900–1300 K range.

The hot-stage microscope (HSM) has been reported as a fast and simple method to estimate viscosity–temperature curves

* Corresponding author.
E-mail address: masainz@icv.csic.es (M.A. Sainz).

0272-8842/$36.00 © 2011 Published by Elsevier Ltd and Techna Group S.r.l.
doi:10.1016/j.ceramint.2010.12.017

within the range $4 < \log \eta < 10$ (η in dPa s). The method was first applied by Scholze [31] for a wide choice of silicate and borosilicate glass compositions. Scholze defined the following points from the optical records of the HSM: the first shrinkage ($\log \eta = 10.0 \pm 0.3$), the maximum shrinkage ($\log \eta = 8.2 \pm 0.5$), the softening ($\log \eta = 6.1 \pm 0.2$), the half ball ($\log \eta = 4.6 \pm 0.1$) and the flow ($\log \eta = 4.1 \pm 0.1$) points, which were used to draw the viscosity–temperature curve. Looking for the optimum conditions to draw glass fibers, De Pablos et al. [32] successfully applied this method to determine the viscosity–temperature curves of different glass compositions in the 1000–1600 K interval. Pascual et al. [33] verified minor differences between the viscosities of three certified standard glasses (E-glass, Pyrex glass and soda-lime-silica float glass) measured by both Scholze's method and the high temperature viscosimeter. In the present work, HSM is used to follow the sintering kinetic of the YAlSiO and YAlSiON powder compositions. HSM and the Scholze's [31] method are attempted for the first time to estimate the viscosity at high temperatures of YAlSiO glasses. Moreover, the glass transition temperature (T_g), the thermal expansion coefficient, density and hardness of these YAlSiO glasses and YAlSiON glass-ceramics are comparatively discussed.

2. Experimental procedure

High purity (>99.8%) commercial powders of SiO_2 (Strem Chemical, France), Al_2O_3 (Alcoa CT-3000SG, Spain) and Y_2O_3 (H.C. Starck, Germany), with a mean particle size of 114, 0.5 and 1 μm, respectively, were used as raw materials. Two nitrogen-free powder mixtures with compositions 6.52 Y–11.95 Al–17.93 Si–63.57 O (*G*) and 10.00 Y–15.00 Al–12.50 Si–62.50 O (*D*) (in at%) were formulated (see Table 1). According to their location in the SiO_2–Al_2O_3–Y_2O_3 phase equilibrium diagram [1–3], composition *G* is in the glass forming zone whereas composition *D* is close to a zone of partial crystallization [10].

To prepare the nitrogen-containing compositions, α-Si_3N_4 powders (E05, UBE Industries, Japan) with 0.5 μm of average particle size were added to the above compositions as the source for nitrogen. The SiO_2/Si_3N_4 molar ratio was fixed to 3:1, maintaining constant the other atomic ratios (Al/Si, Al/Y and Y/Si). These new compositions, labelled as *GN* and *DN*, are also given in Table 1.

The four powder mixtures were attrition milled in isopropyl alcohol for 4 h using Al_2O_3 balls as milling media; afterwards, the slurries were dried at 60 °C and sieved through a 100 μm mesh. The particle size distribution, measured by Laser Diffraction (Mastersizer S, Malvern,UK), ranged from 0.5 to 20 μm for all compositions. The powders were isostatically pressed at 200 MPa into pellets. The two YAlSiO pellets were melted inside a platinum crucible at 1550 °C for 4 h in air, using a heating rate of 5 °C/min; whereas YAlSiON pellets were melted within graphite crucibles at 1800 °C for 2 h under N_2 atmosphere (0.1 MPa), using same heating rate. Subsequently, the glasses were first cooled with a cooling rate of 20 °C/min until a temperature of ≈1000 °C (50 °C above the T_g) annealing for 1 h to remove internal stresses, and afterwards specimens were slowly (5 °C/min) cooled down to room temperature.

Table 1
Elemental composition of the studied glasses and glass-ceramics (at%).

Composition	Y	Al	Si	O	N	Al/Y	Al/Si	Y/Si
G	6.52	11.95	17.93	63.30	–	1.83	0.66	0.36
D	10.00	15.00	12.50	62.50	–	1.50	1.20	0.80
GN	6.93	12.71	19.07	48.55	12.74	1.83	0.66	0.36
DN	10.43	15.65	13.03	52.18	8.71	1.50	1.20	0.80

The density was measured by the Archimedes method at 24 ± 0.5 °C in water. The thermal expansion coefficient was measured in air, at a heating rate of 5 °C/min using a quartz dilatometer (402 EP NETZSCH). The average thermal expansion coefficient was determined in the temperature range of 50–700 °C. On the other hand, glass transition temperature was estimated as the inflection point of the linear expansion versus temperature curves that were recorded in the temperature interval of 200–1200 °C using a high temperature alumina dilatometer (DI-24 Adamel Lhomargy) at a heating rate of 5 °C/min under air atmosphere.

Crystalline phases were identified using X-ray diffraction analyses (D8 Advance Bruker (Germany)) in the 2θ range of 10–80°.

The microstructure of the sintered specimens was observed with the field emission scanning electron microscope (FE-SEM, Model S-4700 HITACHI, Japan). Quantitative elemental composition analyses were obtained by energy-dispersive X-ray spectroscopy (EDS) using the ZAF (atomic number, absorption, fluorescence) correction software and theoretical internal standards. Microanalysis data represented the average of six independent determinations. The Vickers hardness was determined using a microhardness tester (Microhardness tester Type M. Shimadzu, Japan and Zhu 2.5, Zwick/Roell, Germany) with a diamond pyramidal indenter, applying loads between 0.98–4.9 N for 30 s. At least 10 measurements were done for each material. The indented surfaces were observed with an optical microscope (Axiophot H-P1, Carl-Zeiss, Germany) under polarized light conditions, in order to reveal stress birefringence effects.

Sintering of the four compositions was followed with the HSM (Leitz Wetzlar equipment, EM 201). The HSM encompasses image analysis software that automatically computes the specimen geometry during the heating run. The HSM software registers changes in height, width and area of the specimen and from images recorded every 30 s. The tests were done in air, at a heating rate of 10 °C/min up to 700 °C and at 5 °C/min from 700 to 1700 °C. Cylindrical specimens (≈3 mm in height and 2 mm in diameter) were shaped by manually pressing the initial powders and the powdered melts. Then, samples were placed on flat Pt/alumina supports. The temperature was measured with a Pt/Rh (6/30) thermocouple attached to the specimen holder with an error of ±2 °C. The specimen shrinkage was calculated from

Eq. (1):

$$Shrinkage\ (\%) = \frac{A_0 - A_T}{A_0} \times 100 \quad (1)$$

where, A_0 and A_T are the specimen projected areas at initial and T temperatures, respectively. Additionally, the viscosity of the two YAlSiO glasses (G and D) was determined as a function of temperature using Scholze's method [31]. The five viscosity points were geometrically deduced from the HSM image/temperature records: (i) the first shrinkage or sintering, (ii) the maximum shrinkage before softening starts, (iii) the softening point at which the first signal of melting appears, (iv) the half ball point, when the specimen forms a semicircle, and (v) the flow point at which the test piece collapses to a third of its height at the hemisphere state (following standards DIN 51730 1998-04/ISO 540 1995-03-15).

3. Results and discussion

The G and D glasses were highly homogeneous, transparent, colourless and bubble free, as displayed in Fig. 1. Neither optical evidences of phase separation nor crystallisations were observed; furthermore, the amorphous nature of both glasses was confirmed by the corresponding X-ray diffraction patterns, which only showed a broad band.

Conversely, nitrogen containing melts, *DN* and *GN*, were white translucent and grey opaque, respectively. *GN* specimen was difficult to melt and vigorous frothing occurred during melting, probably due to some SiO (g) generation. X-ray diffraction patterns of these compositions showed crystalline phases and an amorphous hump (≈30°) with superimposed low intensity sharp peaks, as depicted in Fig. 2. Crystalline phases identified for *DN* specimens were $YAlO_3$ (YAP) and $SiAl_6O_2N_6$, whereas for *GN* composition, peaks that may be associated to Si_3N_4 or $Si_4Al_2O_2N_6$, as well as Y_2SiAlO_5N and $Y_{10}Al_2Si_3O_{18}N_4$ were detected. SEM micrographs of Fig. 3 show the extensive crystallizations in both glass-ceramics, with coarser crystals (~20 μm) in *DN* than in *GN* (~5 μm) even though the higher crystallization degree of the last one. The EDS analysis allowed the identification of the crystalline phases detected by XRD. The coarse crystals in *DN* (see Fig. 3) had an Al/Y atomic ratio of 0.93 that might be ascribed to the $YAlO_3$ phase; the black acicular crystals presented an Al/Si atomic ratio of 6.2 that is compatible with the $SiAl_6O_2N_6$ phase; and finally, the grey continuous phase (g_3 in Fig. 3) with the Si/Al/Y atomic composition of 14, 11 and 12 (in at %), respectively, would correspond to the amorphous phase.

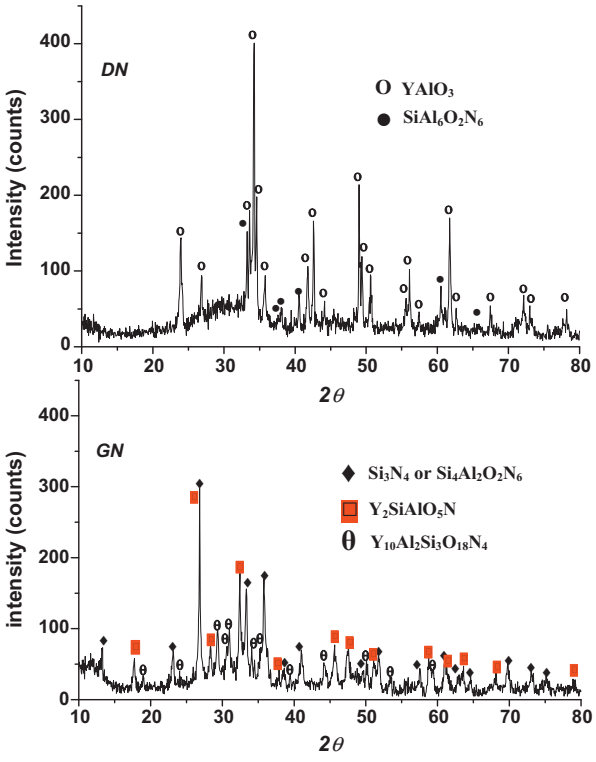

Fig. 2. X-ray diffraction patterns of *GN* and *DN* glass-ceramics.

In the case of the *GN* specimen (see Fig. 3), the microanalyses of the high aspect ratio dark grains gave an Al/Si ratio of about 0.52, similar to the ratio of the $Si_4Al_2O_2N_6$ phase, whereas, the small equiaxed black grains only showed the spectral line of Si, as a result, they should be Si_3N_4 grains, and the surrounding white phase holds Al/Si and Al/Y ratios of 0.6 and 0.3, respectively, which match with the $Y_{10}Al_2Si_3O_{18}N_4$ phase. All these phases were also identified in the XRD pattern of *GN* specimen (Fig. 2). Finally, the continuous grey phase (g_4) in the *GN* image (Fig. 3) should correspond to the glassy phase with a Si/Al/Y composition equal to 16, 12 and 8 (in at%), respectively, which is slightly shifted from the originally formulated (Table 1).

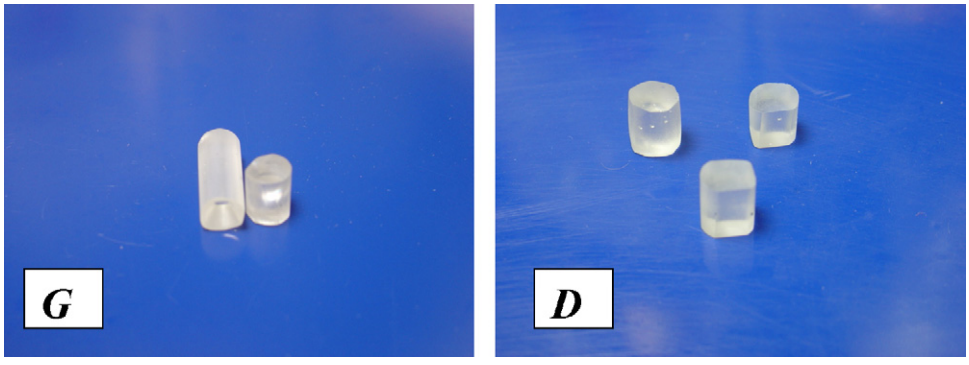

Fig. 1. YAlSiO glasses (G and D) air melted at 1550 °C/4 h(1:1.5).

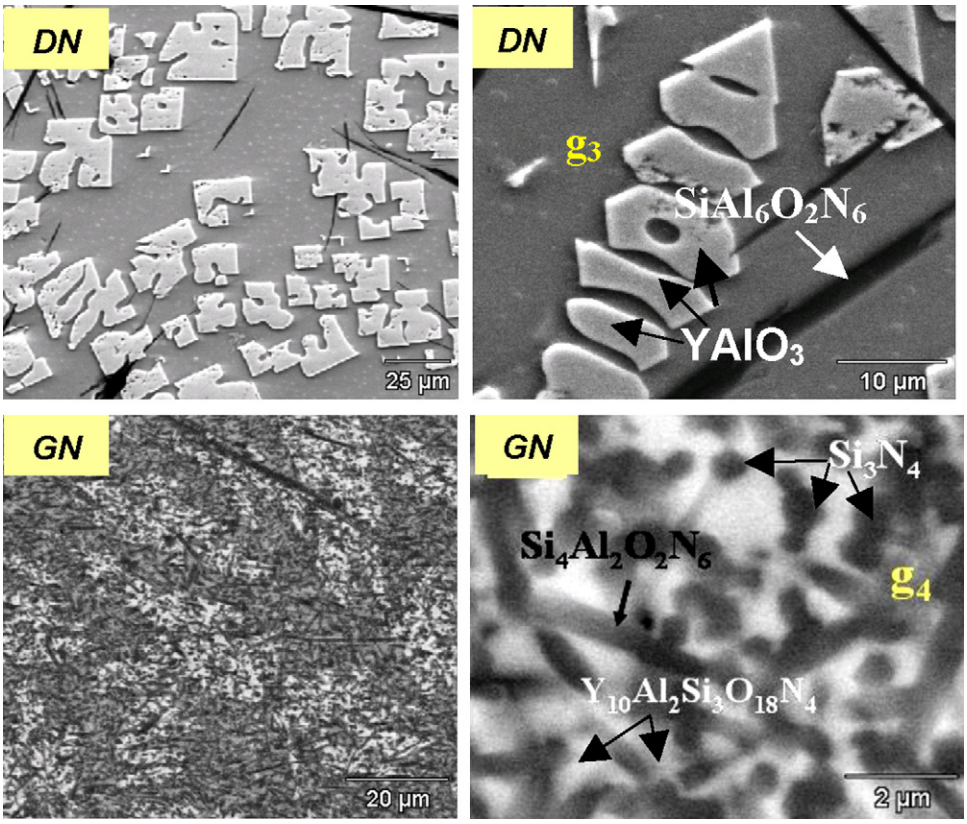

Fig. 3. SEM micrographs of polished *DN* and *GN* glass-ceramics showing extensive crystallizations.

The main properties of the studied glasses and glass-ceramics are collected in Table 2. The densities were 3.08 and 3.42 (g/cm^3) for *G* and *D* glasses, respectively; whereas, the nitrogen containing compositions, *GN* and *DN*, had higher densities, 3.27 and 3.98 (g/cm^3), respectively. The higher density of *D* compared to the *G* glass is due to the higher atomic mass of yttrium and the larger number of Al–O–Si bonds. Conversely, in the *GN* and *DN* glass-ceramics the presence of crystallizations is the determining factor (Fig. 3).

Thermal expansion coefficient of *G* was $4.5 \times 10^{-6}\ K^{-1}$ and slightly higher values were measured for *D* ($6.0 \times 10^{-6}\ K^{-1}$) and *DN* ($5.8 \times 10^{-6}\ K^{-1}$). The thermal expansion coefficient of the *GN* was not determined because of the high number of bubbles in the specimen.

The glass transition temperatures (T_g) of nitrogen free glasses (*G* and *D)* were very similar (935 and 945 °C, respectively) whereas T_g values for *GN* and *DN* were slightly higher, 970 and 1030 °C, respectively.

Fig. 4 shows shrinkage versus temperature data for the powdered glass compositions (*Gg* and *Dg)* and the original raw powder mixtures of same compositions (*G* and *D*). The curves progression for the previously formed glasses are very different from those of the original powder mixtures; in fact, *Gg* and *Dg* glasses show two abrupt steps but *D* and *G* present only one sintering event. In this way, the glasses display the first abrupt shrinkage (∼35%) around the T_g temperature (∼950°), thus corresponding to a classical viscous flow sintering. Between 1050 and 1300 °C, shrinkage practically stops and flow occurs at ≈1400 °C, temperature close to the eutectic point (∼1380 °C) of the SiO_2–Al_2O_3–Y_2O_3 phase equilibrium diagram [1–3]. In these specimens, an expansion is also observed in the 300–1000 °C temperature interval that is higher (7%) for *Dg* than for *Gg* (2.5%), according to their different thermal expansion coefficients (Table 2).

Although similar levels of shrinkage (35%) are observed for the specimens prepared from the starting *G* and *D* powders,

Table 2
Main properties of the different compositions.

Glass	Density (g cm^{-3})	T_g (°C)	Viscosity (Pa s) T (K) = 1500	Hardness (GPa)	$\alpha_{(50–700\ °C)} \times 10^{-6}\ K^{-1}$
G	3.08	935	7.2 ± 0.2	6.6 ± 0.6	4.5 ± 0.5
D	3.42	945	7.7 ± 0.2	8.1 ± 0.6	6.0 ± 0.5
GN	3.27	970	–	13.2 ± 0.9	–
DN	3.98	1030	–	11.7 ± 0.9	5.8 ± 0.5

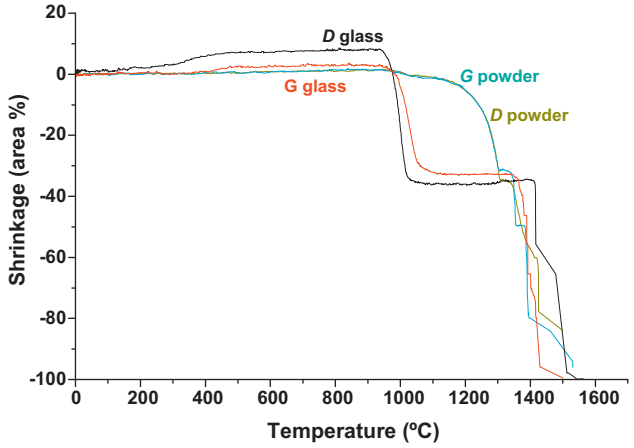

Fig. 4. Sintering curves for *G* and *D* compacts prepared from both the powdered glasses and starting powders.

compared to *Gg* and *Dg*, sintering occurred at higher temperatures (above 1200 °C) and at lower rates, probably under the presence of progressive amounts of liquid phase. In this case, the initial expansion observed for the glass specimens is not detected. Melting occured at same temperature for all composition, as it can be expected.

Shrinkage curves versus temperature for all the starting powder mixtures (*G*, *D*, *GN* and *DN*) are compared in Fig. 5. The addition of Si_3N_4 hindered densification in GN and DN, shifting their shrinkage starting point about 200 °C. This retard is more significant for *GN* according to its higher Si_3N_4 content. Melting was not clearly detected in the case of *GN* and *DN* and instead, a sharp expansion occurred, possibly due to both the formation of bubbles and decomposition of the Si_3N_4 phase in the melt. Two competitive phenomena, both decreasing the surface energy of powder compacts, can take place during liquid phase sintering, i.e. densification and crystallization, which defines the final shrinkage behavior of glass-ceramics. In the present work for *D* and *G*, shrinkage temperatures are much lower than crystallization temperatures, thus producing well sintered glasses, whereas, for *DN* and *GN* compositions,

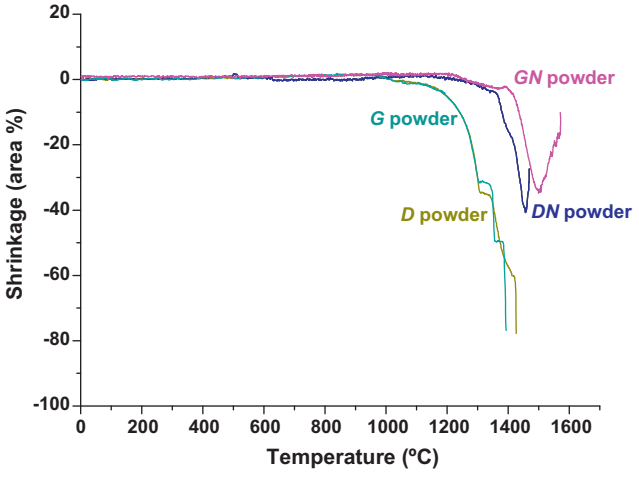

Fig. 5. Shrinkage versus temperature curves for *G*, *D*, *GN* and *DN* compacts prepared from starting powders.

crystallization occurred during densification leading to porous glass-ceramics.

Fig. 6 shows a selected sequence of HSM images corresponding to the specimens contours at defined viscosity points for *G* and *D* glasses. At the half ball point, a relative high wetting angle, which infers a high surface tension, was observed for both compositions (Fig. 6d).

The experimental viscosity–temperature data for *G* and *D* glasses (Fig. 7) were adjusted to the Vogel–Fulcher–Tammann–Hesse, VFTH [34–36] equation:

$$\mathrm{Log}\,\eta = A + \frac{B}{T - T_o} \tag{2}$$

where *A*, *B* and T_0 are constants for each glass. VFTH fittings (lines in Fig. 7) gave an *A* of -5.5 ± 0.5 (η in Pa s). For glasses of different sources, Nascimento and Aparicio [37] calculated *A*, *B* and T_0 by VFTH fittings and they also got a distribution of *A* values near -5 (η in Pa s). The *B* and T_0 values for *D* and *G* glasses obtained from Eq. (2) once *A* was fixed to -5, are comparable for both glasses (see Table 3), suggesting that they must have similar network structures, although the slightly higher *B* and lower T_0 in *D* than in *G* would corresponds to the lower polimerization degree in *G* glasses [38]. In all cases, the fittings gave reasonable regression coefficients (≈0.96 to 0.99). At any given temperature viscosity was slightly higher for *D* than for *G glass* as seen in Fig. 7; the values at 1500 K are given in Table 2.

VFTH analysis is a useful tool for describing the viscosity–temperature dependence of strong, moderate and fragile glasses [39,40] above T_g. Several authors [41–43] have reported a correlation between *B* and T_0 parameters of VFTH analysis, pointing that ''stronger glasses'' present higher *B* parameters and lower T_0, in opposition to the ''fragile'' ones. The strength of these glasses is directly related to the stability of the system at temperatures above the glass transition. According to this, *D* and *G* glasses would present a slightly higher stability and stronger behaviour than lithia, soda and potassium silicate/borate systems [39,44].

The average Vickers hardness of the *G* and *D* glasses were 6.6 ± 0.6 and 8.1 ± 0.6 GPa, respectively (Table 2). Fig. 8 shows some examples of Vickers indentations at different loads. Cracks were not observed at low loads (0.98 N) although at 1.96 N the typical Vickers indentation radial crack geometry in G was produced. Stress birefringence effects around the indentation cracks are significant at higher loads (4.9 N), which gives indication that lateral cracks grew during unloading. Hardness (Table 2) is related to the degree of cross-linking in the glass network, as it will be discussed later. In this way, the increase in the Y/Si ratio for the glasses ($D > G$) produces the slight increase in hardness of *D*. Hardness values for the N containing glass-ceramics were: 13.2 ± 0.9 and 11.7 ± 0.9 GPa for *GN* and *DN* compositions, respectively, higher than those of the parent YAlSiO glasses. The remarkable increase in hardness of the *GN* glass-ceramics is mainly attributable to the extensive crystallization observed in this specimen (Fig. 3). In the case of *DN*, hardness was measured on the glass matrix (Fig. 9a) and, then, it can be inferred an increase in hardness

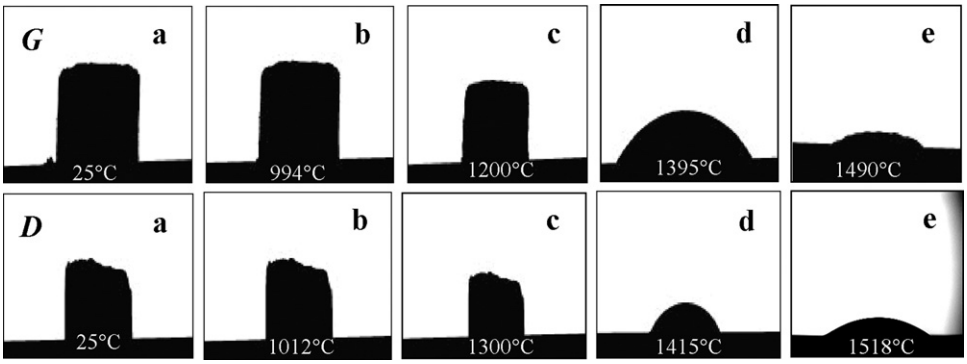

Fig. 6. HSM images showing the geometry of the characteristic viscosity points as defined by Scholze[31] for *G* and *D* glasses: (a) initial shape, (b) first shrinkage, (c) softening point, (d) half ball point and (e) flow point.

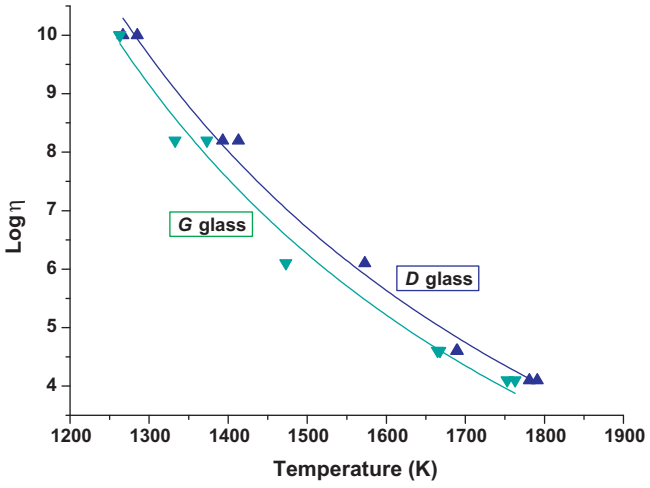

Fig. 7. Viscosity versus temperature plots of *G* and *D* compacts prepared from powdered glasses Lines are the VFTH fittings.

with inclusion of N atoms [12] in the glass network; however, it should be pointed out that hardness was significantly higher (>19 GPa) when it was measured on areas containing crystallizations. In that case, crack deflection was observed (Fig. 9b). As hardness gives an idea of the strength of the glass bond, the studied glasses must have stronger bonds than fused silica ($H \approx 5.9$ GPa) [45], which makes them particularly suitable for applications under abrasive conditions. Moreover, the crystallization propensity of *DN* and *GN* glasses opens new prospects for others applications such as protective metal coatings [10] where high thermal expansion coefficients and hardness are required conditions.

A progressive degree of cross-linking of the glass network is proposed according the following order: $G < D < GN < DN$. Differences in properties of *G* and *D* glasses can be explained by the distinct connectivity of their glass-networks, as consequence of the *v*ariations in the Al/Si and Y/Si ratios

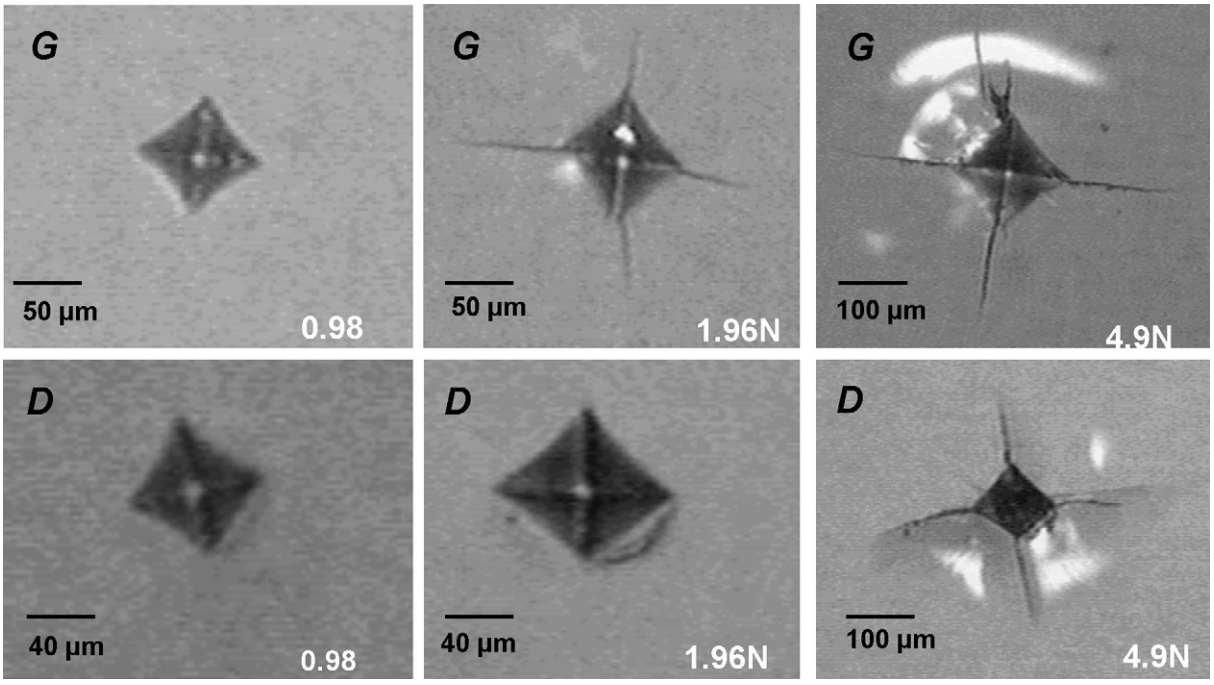

Fig. 8. Optical micrographs of Vickers indentations in *G* and *D* glasses at given loads (0.98–4.9 N).

Table 3
Fitting parameters of the VFTH equation(2).

Composition	Constant[a] of VFTH equation		Regression coefficients
	B (K)	T_0 (K)	
G	11014	522	0.96
D	11630	506	0.99

[a] B and T_0 are calculated from linear regression analysis (A was fixed as -5, η in Pa s units).

[9,15,41]. In fact, as it is discussed below, the high Al/Si ratio of D composition and its larger Y/Si ratio compared with G account for its superior values of hardness, viscosity and T_g (Table 2) owing to the increase of the glass network compactness.

Aluminium ions (Al^{3+}) may act as network formers [2] assuming the (AlO_4) coordination or even as modifiers at elevated Al/Si ratios (>1), with 5- and 6-fold (AlO_6) coordination [4]. In the case of G glass, with an Al/Si ratio of 0.66, only 4-fold tetrahedral coordination should be expected, and therefore, three aluminium units should share a single triply charged yttrium ion to maintain local charge neutrality. In the case of D glass, which presents Al/Si ratio > 1 (Table 2), small percentage of aluminium tricluster as well as 5- and 6-fold coordinated aluminium ions may also exist [4,46].

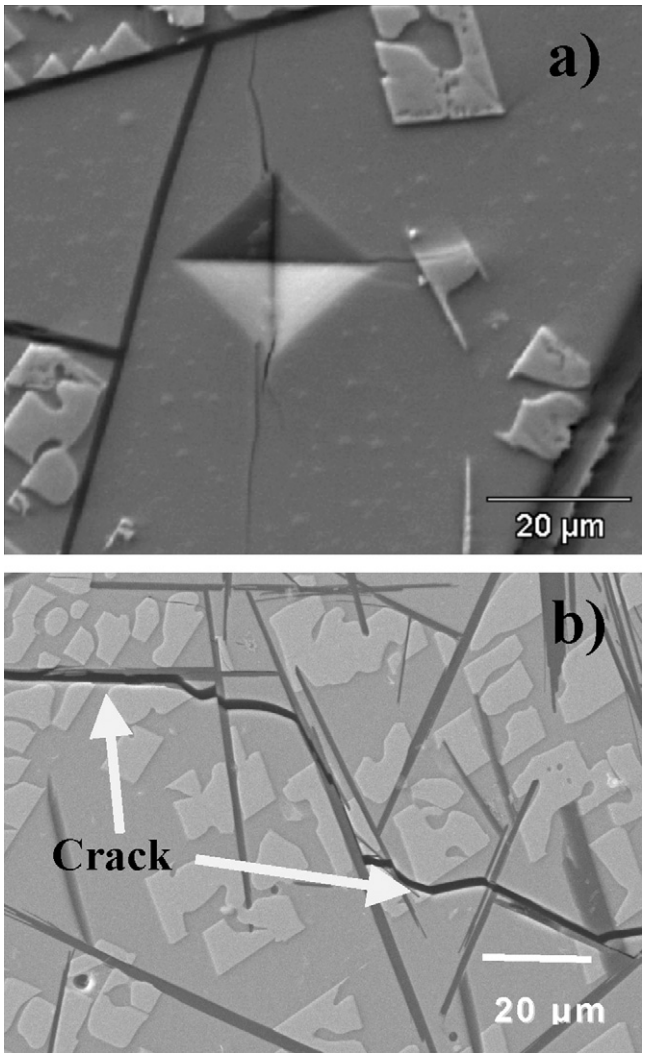

Fig. 9. SEM micrographs showing details of a Vickers indentation (a) and a deflected crack path (b) for the *DN* glass-ceramics.

Furthermore, yttrium ion (Y^{3+}) always performs as a network modifier and a charge compensating ion. In this way, it may occupy the space between Si–$(O,N)_x$ and Al–$(O,N)x$ tetrahedra, which will increase the glass network connectivity and the cross-linking. This effect is more important in the case of D glass with a higher Y/Si content than G.

Conversely, the higher thermal expansion coefficient of D versus G composition (see Table 2) cannot be explained by its more compact network [47] but by the increase in the anharmonicity of the thermal vibrations due to the larger content of Y^{3+} ions (in D glass) which generates an increase of the bonds asymmetry [48].

Regarding Si_3N_4 containing compositions, as nitrogen substitutes oxygen in the glass network [2,11,42] and is covalently bonded to silicon, a more rigid and highly cross-linked structure generates that improves properties of the nitrogen containing glasses. The number of oxygen bonded to two silicons can be estimated from the glass composition using the next expression [13]:

$$n_{\mathrm{Si-O-Si}} = 2(4 - r) \tag{3}$$

where r is the O/Si atomic ratio. Eq. (3) gives values of $n_{\mathrm{Si\text{-}O\text{-}Si}} \geq 1$ for *GN*, whereas it is zero for *DN*, which foresees the existence of disilicate groups only in *GN* indicating the more weak bonds in this composition.

4. Conclusions

New glasses and glass-ceramics materials in the SiO_2–Al_2O_3–Y_2O_3–Si_3N_4 system with potential application as protective coatings for metallic components have been developed. Homogeneous glasses have been obtained for the YAlSiO compositions and glass-ceramics when Si_3N_4 was added to the previous mixtures. Properties and viscosity of the different compositions have been explained by the degree of cross-linking of the glass network, considering the Al/Si and Y/Si ratios and the nitrogen content as well. The remarkably increase in hardness of these glass-ceramics is mainly associated to the presence of crystallizations.

Hot stage microscopy has been proved to be a rather simple and reliable way to analyse the sintering and viscosity behaviours of these types of materials. Viscosity–temperature data for YAlSiO glasses have been measured up to temperatures as high as 1800 K and experimental values fit to the VFHT equation giving similar values of parameters B and T_0 for both glasses.

Acknowledgements

This work was funded by MICINN (Ministry of Science and Innovation, Spain) under project MAT 2006-07118, MP2008-1732 and MAT 2009-09600. Financial support of NRC-CSIC Cooperation program (project 2007CA003) is also recognized.

References

[1] M.J. Hyatt, D.E. Day, Glass properties in the yttria–alumina–silica system, J. Am. Ceram. Soc. 70 (10) (1987) C283–287.

[2] J.E. Shelby, S.M. Minton, C.E. Lord, et al., Formation and properties of yttrium aluminosilicate glasses, Phys. Chem. Glasses 33 (3) (1992) 93–98.

[3] U. Kolitsch, H.J. Seifert, T. Ludwig, F. Aldinger, Phase equilbria and crystal chemistry in the Y_2O_3–Al_2O_3–SiO_2 system, J. Mater. Res. 14 (2) (1999) 447–455.

[4] J.T. Kohli, J.E. Shelby, J.S. Frye, A structural investigation of yttrium aluminosilicate glasses using Si-29 and Al-27 magic angle spinning nuclear-magnetic-resonance, Phys. Chem. Glasses 33 (3) (1992) 73–78.

[5] K. Oda, T. Yoshio, Properties of Y_2O_3–Al_2O_3–SiO_2 glasses as a model system of grain-boundary phase of Si_3N_4 ceramics. 2. Leaching characteristics, J. Ceram. Soc. Jpn. 99 (7) (1991) 1150–1152.

[6] A. Makishima, Y. Tamura, T. Sakaino, Elastic-moduli and refractive-indexes of aluminosilicate glasses containing Y_2O_3, La_2O_3, and TiO_2, J. Am. Ceram. Soc. 61 (5-6) (1978) 247–249.

[7] K. Morita, A. Umezawa, S. Yamato, A. Makishima, Surface-roughness of yttria-containing aluminosilicate glass-ceramics as indicative of their machinability, J. Am. Ceram. Soc. 76 (7) (1993) 1861–1864.

[8] J. Johnson, R. Weber, M. Grismsditch, Thermal and mechanical properties of rare earth aluminate and low-silica aluminosilicate optical glasses, J. Non-Cryst. Solids 351 (2005) 650–655.

[9] H. Kaplandiedrich, G.H. Frischat, Properties of some oxynitride glass-fibers, J. Non-Cryst. Solids 184 (1995) 133–136.

[10] M.A. Sainz, M.I. Osendi, P. Miranzo, Protective Si–Al–O–Y glass coatings on stainless steel in situ prepared by combustion flame spraying, Surf. Coat. Technol. 202 (2008) 1712–1717.

[11] R.E. Loehman, Preparation and properties of oxynitride glasses, J. Non-Cryst. Solids 56 (1–3) (1983) 123–134.

[12] D.R. Messier, A. Broz, Microhardness and elastic-moduli of Si–Y–Al–O–N glasses, J. Am. Ceram. Soc. 65 (8) (1982) C123–125.

[13] H. Lemercier, T. Rouxel, D. Fargeot, et al., Yttrium SiAlON glasses: structure and mechanical properties – elasticity and viscosity, J. Non-Cryst. Solids 201 (1–2) (1996) 128–145.

[14] S. Hampshire, E. Nestor, R. Flynn, et al., Yttrium oxynitride glasses – properties and potential for crystallization to glass-ceramics, J. Eur. Ceram. Soc. 14 (3) (1994) 261–273.

[15] S. Hampshire, Oxynitride glasses, their properties and crystallisation – a review, J. Non-Cryst. Solids 316 (1) (2003) 64–73.

[16] M.A. Sainz, P. Miranzo, M.I. Osendi, Silicon nitride joining using silica and yttria ceramic interlayers, J. Am. Ceram. Soc. 85 (4) (2002) 941–946.

[17] D.R. Clarke, N.J. Zaluzec, R.W. Carpenter, The intergranular phase in hot-pressed silicon-nitride. 1. Elemental composition, J. Am. Ceram. Soc. 64 (10) (1981) 601–607.

[18] S. Hampshire, The role of additives in the pressureless sintering of nitrogen ceramics for engine applications, Metals Forum. 7 (3) (1984) 162–170.

[19] M.K. Cinibulk, G. Thomas, S.M. Johnson, Grain-boundary-phase crystallization and strength of silicon-nitride sintered with a YSiAlON glass, J. Am. Ceram. Soc. 73 (6) (1990) 1606–1612.

[20] D.H. Kim, C.H. Kim, Toughening behavior of silicon-carbide with additions of yttria and alumina, J. Am. Ceram. Soc. 73 (5) (1990) 1431–1434.

[21] D.S. Wilkinson, Creep mechanisms in multiphase ceramic Materials, J. Am. Ceram. Soc. 81 (2) (1998) 275–299.

[22] W.E. Luecke, S.M. Wiederhorn, A new model for tensile creep of silicon nitride, J. Am. Ceram. Soc. 82 (10) (1999) 2769–2778.

[23] P.A. Walls, M. Ueki, Joining sialon ceramics using composite beta-sialon glass adhesives, J. Am. Ceram. Soc. 75 (9) (1992) 2491–2497.

[24] S.J. Glass, F.M. Mahoney, B. Quillan, J.P. Pollinger, R.E. Loehman, Refractory oxynitride joints in silicon nitride, Acta Mater. 46 (7) (1998) 2393–2399.

[25] M. Gopal, L.C. De Jonghe, G. Thomas, Silicon nitride: from sintering to joining, Acta Mater. 46 (7) (1998) 2401–2405.

[26] R.-J. Xie, M. Mitomo, Joining of silicon nitride ceramics for high-temperature applications, J. Mater. Res. 15 (1) (2000) 136–141.

[27] N. Saito, K. Kai, S. Furusho, et al., Properties of nitrogen-containing yttria–alumina–silica melts and glasses, J. Am. Ceram. Soc. 86 (4) (2003) 711–716.

[28] T. Rouxel, M. Huger, J.L. Besson, Rheological properties of Y–Si–Al–O–N glasses – elastic-moduli, viscosity and creep, J. Mater. Sci. 27 (1) (1992) 279–284.

[29] P.F. Becher, M.K. Ferber, Temperature-dependent viscosity of SiREAl-based classes as a function of N: O and RE: Al ratios (RE = La, Gd, Y, and Lu), J. Am. Ceram. Soc. 87 (7) (2004) 1274–1279.

[30] S. Hampshire S, M.J. Pomeroy, Effect of composition on viscosities of rare earth oxynitride glasses, J. Non-Cryst. Solids 344 (1–2) (2004) 1–7.

[31] H. Scholze, Influence of the viscosity and surface tension on hot-stage microscopy measurements on glasses, Ver. Dtsch. Keram. Ges. 391 (1962) 63–68.

[32] A. De Pablos, A. Duran, M.I. Nieto, Adjusting of laboratory filature furnace for obtaining fibreglass, Bol. Soc. Esp. Ceram. Vidr. 36 (5) (1997) 517–523.

[33] M.J. Pascual, L. Pascual, A. Duran, Determination of the viscosity–temperature curve for glasses on the basis of fixed viscosity points determined by hot stage microscopy, Phys. Chem. Glasses 42 (1) (2001) 61–66.

[34] H. Vogel, Temperature dependence of viscosity of melts, Physik Z. 22 (1921) 645–646.

[35] G.S. Fulcher, Analysis of recent measurements of the viscosity of glasses, J. Am. Ceram. Soc. 8 (1925) 339–355.

[36] G. Tammann, W. Hesse, Temperature dependence of viscosity of melted supercooled liquids, Z. Anorg. Chem. 156 (1926) 245–247.

[37] M.L.F. Nascimento, C. Aparicio, Viscosity of strong and fragile glass-forming liquids investigated by means of principal component analysis, J. Phys. Chem. Solids 68 (1) (2007) 104–110.

[38] I. Avramov, Viscosity in disordered media, J. Non-Cryst. Solids 351 (40–42) (2005) 3163–3173.

[39] C.A. Angell, Relaxation in liquids, polymers and plastic crystals – strong fragile patterns and problems, J. Non-Cryst. Solids 131 (1) (1991) 13–31.

[40] R. Bohmer, K.L. Ngai, C.A. Angell, et al., Nonexponential relaxations in strong and fragile glass formers, J. Chem. Phys. 99 (5) (1993) 4201–4209.

[41] S. Kumar, K.J. Rao, Viscosity scaling of glass forming liquids on the basis of fragility, Chem. Phys. Lett. 382 (1–2) (2003) 87–91.

[42] N.H. Ray, Composition – property relationships in inorganic oxide glasses, J. Non-Cryst. Solids 15 (3) (1974) 423–434.

[43] K.H. Jack, Sialons and related nitrogen ceramics, J. Mater. Sci. 11 (6) (1976) 1135–1158.

[44] C.A. Angell, Perspective on the glass-transition, J. Phys. Chem. Solids 49 (8) (1988) 863–871.

[45] O.V. Mazurin, M.V. Streltsina, T.P. Shvaiko-Shvaikovskaya, in: Handbook of Glasses Data, Pt A, Silica Glass and Binary Silicate Glasses, Elsevier, New York, 1983, p. 115.

[46] B.O. Mysen, P. Richet, Silicate Glasses and Melts, Elsevier, Amsterdam, 2005, 283-287.

[47] S.N. Salama, S.M. Salman, Contribution of manganese oxide to the thermal-expansion of some silicate-glasses and their crystalline solids, Thermochim. Acta 191 (1) (1991) 187–199.

[48] J. Zarcycki, Glasses and Amorphous Material, Materials Science and Technology, vol. 9, Weinheim, 1991.